Typeset using jjap.cls <ver.1.0.1>

High Coupling Efficiency of Microcavity Organic Light-Emitting Diode with Optical Fiber for as Light Source for Optical Interconnects

Takeshi FUKUDA*, Bin WEI[1], Masakazu OHASHI, Musubu ICHIKAWA[1] and Yoshio TANIGUCHI[1]

Applied Electronics Technology Department, Optics and Electronics Laboratory, Fujikura Ltd., 1440, Mutsuzaki, Sakura, Chiba, 285-8550, Japan

[1]*Department of Functional Polymer Science, Faculty of Textile Science and Technology, Shinshu University, 3-15-1, Tokida, Ueda, Nagano, 386-8567, Japan*

(Received)

We investigated the directional characteristics of the electroluminescence (EL) from microcavity organic light-emitting diodes (MOLEDs) to examine applicability of these diodes as a light source for optical interconnects. By measuring the angular dependence of a EL emission, we estimated the coupling efficiency between a MOLED and an optical fiber. The coupling efficiency was enhanced by 1.4-fold compared with that of a non cavity organic light-emitting diode (OLED) , and reached 85 % for an optical fiber with a numerical aperture (NA) of 0.5. The current efficiency of the MOLED also increased optimizing the device structure, and its maximum was 18.4 cd/A.

KEYWORDS: OLED, microcavity structure, tris (8-hydroxyquinolato) aluminum, optical interconnect, light source

*E-mail address: fukuda@lab.fujikura.co.jp

1. Introduction

In recent years, several breakthroughs have led to significant enhancements in the performance of organic light-emitting diodes (OLEDs) , such as the improvement in charge-carrier balance,[1,2] the development of low-work function electrode materials,[3] and the realization of high carrier mobility and high EL quantum efficiency in organic light-emitting layers,[4] high fluorescence efficiency emitting materials,[5–7] and phosphorescence emitting materials.[8] Therefore, the internal quantum efficiency of OLEDs has been optimized gradually close to the theoretical limit.[6]

On the other hand, only a small fraction of total photons generated inside the emitting layer are generally usable, because of the internal reflection and the confinement effects of high-refractive-index layers.[9] For an OLED with a sandwiched structure between a metal reflector and a transparent anode, the fraction of light generated in the organic layer and escaping from the substrate into the air can be estimated to be $1/(2 \times n_{org}^2)$. Where n_{org} is the refractive index of the organic layer. Therefore, we can determine that the light coupling efficiency of OLEDs is typically only 20 % under the assumption of $n_{org} = 1.6$. The rest of the light either is absorbed by the metal cathode and the polaron produced by applying voltage or escapes through waveguide mode of the substrate.[10–12]

The use of microcavity structures in OLEDs is an effective approach to enhancing extraction efficiency. Because a microcavity structure concentrates spontaneous emission photons to be perpendicular to a cavity structure, the emission intensity of a cavity device increases as compared with the non cavity device.[13,14] We can also realize spectrally narrowed[13,15] and highly directional EL emissions.[15–17] Therefore, strongly directed pure RGB ELs are emitted from a microcavity organic-light-emitting diode (MOLED) .[15] These effects are useful as not only OLED displays but also light sources for optical interconnects.

To date, OLEDs that intrinsically possess a rapid time response have been investigated as light sources for optical interconnects.[18–20] OLED light sources have already demonstrated a transmission speed of 100 MHz.[18] However, the optical coupling between OLED light sources and optical fibers is crucial in achieving high efficiency signal transmission,

because optical signals from OLEDs should enter into an optical fiber. Therefore, it is essential to optimize the directional characteristics of EL from an OLED. Furthermore, there is as yet no report on the coupling efficiency between OLEDs and fibers, to the best of our knowledge. Because the EL distribution of conventional OLEDs is usually close to the Lambertian distribution, the coupling efficiency of OLEDs with optical fibers decreases in contrast to that in the case of semiconductor lasers. In this study, we investigated the angular dependence of EL from several MOLEDs with different structures, and also evaluated the coupling efficiency between a MOLED and an optical fiber on the basis of its dependence on angle.

2. MOLED Design

In MOLEDs, a microcavity structure is defined by a metal cathode and a distributed Bragg reflector (DBR) formed on a glass substrate. We used MgAg layer as the metal cathode and several SiO_2 and Ta_2O_5 pairs of SiO_2 and Ta_2O_5 quarter wavelength layers as the DBR. The cavity length is expressed by[13,15)]

$$L(\lambda) = \frac{\lambda}{2}\left(\frac{n_{eff}}{\Delta n}\right) + \sum_j n_j L_j + \left|\frac{\phi_m}{4\pi}\lambda\right), \tag{2.1}$$

where n_{eff} and Δn are the effective refractive index of the DBR and the refractive index difference between SiO_2 and Ta_2O_5, and the n_j and L_j are the refractive index and the thickness of the organic and indium tin oxide (ITO) layers, respectively. ϕ_m is the phase shift at the metal cathode expressed by[21)]

$$\phi_m = \arctan\left(\frac{2n_s k_m}{n_s^2 - n_m^2 - k_m^2}\right), \tag{2.2}$$

where n_s is the refractive index of the organic layer in contact with the metal cathode, and n_m and k_m are the real and imaginary parts of the refractive index of the metal cathode, respectively. Cavity modes are given by the relationship $m\lambda = 2L(\lambda)$, where m is the mode index. The mode index can be adjusted by varying the cavity length L (λ) .

3. Experiment

We fabricated three kinds of MOLED devices (Fig. 1) . The mode indexes are 4 for devices A and C, and 5 for device B. First, we prepared a DBR consisting of several pairs

of SiO_2 and Ta_2O_5 and an indium tin oxide (ITO) anode on a glass substrate. The DBR and ITO layers are deposited by electron beam deposition and RF sputtering, respectively. The thicknesses of the SiO_2 and Ta_2O_5 layers were set to be equal to the quarter optical lengths of a center wavelength (510 nm) ; they are 86.32 and 56.85 nm, respectively. The number of the SiO_2/Ta_2O_5 pair varied from 1 to 7 with a chang in the reflectivity of the DBR. The thicknesses of the ITO anode are 100 nm for devices A and C, and 150 nm for device B. The prepared glass substrate was cleaned in deionized water, detergent, and isopropyl alcohol sequentially under ultrasonic waves, and then treated with 50 W oxygen plasma for 5 min just before use.

Next, we deposited organic layers and a metal cathode using a conventional vacuum deposition system at a base pressure of below 5.0×10^{-6} Torr. Each organic layers consisted of 4,4'-bis [*N*- (1-napthyl) -*N*-phenyl-amino] -biphenyl (α-NPD) as a hole transport layer (HTL) , tris (8-hydroxyquinoline) aluminum (Alq_3) doped with 0.4- wt% coumarin 6 (for devices A and B) or rubrene (for device C) as a light-emitting layer (EML) , Alq_3 as an electron transport layer (ETL) , LiF as an electron injection layer (EIL) , and MgAg (9:1 mol ratio) as a cathode. The thicknesses of all the layers are shown in Fig. 1. Figure 1 also shows the chemical structures of the dopants. The deposition rates ranged from 0.08 to 0.12 nm/s for the ETL and HTL, 0.01 to 0.02 nm/s for the EIL, and 5.0 nm/s for the EML and cathode. The active area was 2×2 mm^2.

We measured luminance-current density-voltage characteristics with a source measure unit (HP4140B, Hewlett-Packard) and a luminance color meter (BM-7, TOPCON) . The color meter was placed normal to the test device to measure the front luminance at a solid angle of 1 deg.

4. Results and Discussion

Figure 2 shows the reflection spectra of the DBRs. As clearly shown in Fig. 2, the center wavelengths all the DBRs are about 550 nm and the reflectivity at the center wavelength increases with increasing number of SiO_2 and Ta_2O_5 pairs. The DBRs have a sufficiently broad stop band to confine the entire EL emission except for the cavity resonance wavelength.

Figures 3(a)-3(c) show the current efficiencies defined here as the ratio of the front luminance and the current density, and the full width at half maximum (FWHM) of the EL spectra of all the devices as functions of the number of SiO_2 and Ta_2O_5 pairs. Current efficiency was measured at a current density of 60 mA/cm^2. Although the non cavity OLEDs (number of pairs, 0) exhibited a spectrally broad emission with FWHMs of 64.8 nm for device A, 88.0 nm for device B, and 67.0 nm for device C, the FWHMs decreased with increasing number of SiO_2 and Ta_2O_5 pairs and then to minimum values of 8.7 nm for device A, 6.0 nm for device B, and 9.3 nm for device C. As shown in Figs. 3(a) and 3(b), current efficiency decreased with increasing number of SiO_2 and Ta_2O_5 Macro 1s for devices A and B which had the same EML (coumarin-6-doped Alq_3).

On the other hand, the current efficiency of device C (rubrene-doped Alq_3 EML device) initially increased up to 18.4 cd/A when the number of SiO_2 and Ta_2O_5 pairs was 2, and then decreased with an increase in that number. A microcavity causes photons of spontaneous emission to be concentrated perpendicular to itself. Therefore, current efficiency can increase with increasing number of reflections of the DBR. The decrease in current efficiency can be explained as follows: The number of such reflections at the metal cathode increases using more reflective DBRs.[16] Metal mirrors have some absorption loss due to their electric resistivity; such absorption loss increases with the boosting reflectivity of a DBR. Thus, the combination of concentration and absorption loss is led to the result shown in Fig. 3(c).

On the other hand, current efficiency monotonically decreased for devices A and B, as shown in Figs. 3(a) and 3(b), respectively. Coumarin-6-doped Alq_3, which is used as EML of devices A and B, absorbed the EL emission itself, because it has a higher absorption coefficient than rubrene-doped Alq_3, as clearly shown in Fig. 4. In addition, the total propagation length of the EL emission in the organic layer for MOLEDs increased compared with that for non cavity conventional OLEDs. Therefore, current efficiency monotonically decreased with increasing reflectivity of the DBR for devices A and B.

We also measured the angular dependence of EL spectra from the MOLEDs. Figure 5 shows the EL spectra of device A with a 4-SiO_2/Ta_2O_5-pair DBR together with those from another device A without a DBR, as shown in Fig. 5(b), where the mode index of device

A is 4. For the device with a DBR, the resonance wavelengths as the angle against normal to the device increases, and peak intensity decreases gradually. Meanwhile, another peak in the red region appears, as shown in the inset of Fig. 5(a).

Figure 6 shows the angular dependence of the EL spectra of device B whose mode index is 5. Resonance wavelength is also shifted toward shorter wavelengths as the detection angle is tilted, and another peak at approximately 630 nm also appears. The intensity of the other peak is significantly higher than that of the peak of device A [see the inset of Fig. 5(a)], and is independent of angle. On the other hand, the peak intensity at the resonance wavelength decreased with increasing angle. In other words, the relative intensity of the peak at approximately 630 nm increases with tilting angle. Therefore, the directionality of device B with a mode index of 5 is lower than that of device A. Note that the other peak at approximately 630 nm means a higher mode of resonance.[13)] Figure 7 shows the angular dependence of EL spectra for devices A, B, and C. The EL spectra were measured with a luminance color meter by tilting the samples from -80 deg to 80 deg in steps of 5 deg.

Finally, we estimated the coupling efficiency between an OLED and an optical fiber to examine applicability of OLEDs as a light source for optical interconnects. Figure 8 shows the coupling efficiency as a function of the number of SiO_2/Ta_2O_5 pairs for each device. The efficiency was calculated from the angular dependence of EL intensity shown in Fig. 7, where the numerical aperture (NA) of a coupled optical fiber was assumed to be 0.5. In devices A and C with a mode index of 4, coupling efficiency initially increases and then decreases as the number of SiO_2 and Ta_2O_5 pairs increases. In particular, the coupling efficiency of device A reaches 85 % when the number of SiO_2/Ta_2O_5 pair is 3. On the other hand, the coupling efficiency of the device B monotonically decreased with increasing number of such SiO_2 and Ta_2O_5 pairs. This is because, the relative intensity of the mode index peak higher than the resonance wavelength increases as mentioned before.

These results indicate that a mode index of 4 is necessary to realize the high coupling efficiency of MOLEDs with an optical fiber. By optimizing the reflectivity of the DBR, the coupling efficiency of what was enhanced by 1.4-fold with that of a non cavity OLED.

5. Conclusions

We investigated high directionality MOLEDs to evaluate their applicability as light sources for optical interconnects. The directionality of the MOLEDs is improved by optimizing the reflectivity of the DBR, developing organic materials of the EMLs, and increasing the mode index of the cavity. The coupling efficiency between a MOLED and an optical fiber was calculated from the angular dependence of the EL spectra. The dependence of current efficiency on the reflectivity of the DBR has been investigated for a coumarin-6 or rubrene-doped Alq_3 EML device. The current efficiency increased by optimizing the reflectivity of the DBR.

References

1) J. Kido and T. Matsumoto: Appl. Phys. Lett. **73** (1998) 2866.

2) L. S. Hung, C. W. Tang, and M. G. Mason: Appl. Phys. Lett. **70** (1997) 152.

3) I. D. Parker: J. Appl. Phys. **75**, (1994) 1656.

4) L. S. Hung and C. H. Chen: Mater. Sci. Eng. R **39** (2002) 143.

5) C. W. Tang, S. A VanSlyke, and C. H. Chen: J. Appl. Phys. **65** (1989) 3610.

6) C. Adachi, M. A. Baldo, M. E. Thompson, and S. R. Forrest: J. Appl. Phys. **90** (2001) 5048.

7) Y. Cao. I. Parker, G. Yu, Z. Gang, and A. Heeger: Nature (London) **397** (1999) 414.

8) M. A. Baldo, S. Lamansky, P. E. Burrows, M. E. Thompson, and S. R. Forrest: Appl. Phys. Lett. **75** (1999) 4.

9) A. Chutinan, K. Ishikawa, T. Asano, M. Fujita, and S. Noda: Org. Electron. **6** (2005) 3.

10) T. Tsutsui, E. Aminaka, C. P. Lin, and D.-U. Kim: Philos. Trans. R. Soc. London, Ser. A **355** (1997) 801.

11) N. Patel, K. S. J. Cina, and H. Burroughes: IEEE J. Sel. Top. Quantum Electron. **8** (2002) 346.

12) K. Meerholz and D. C. Muller: Adv. Funct. Mater. **11** (2001) 346.

13) A. Dodablapur, L. J. Rothberg, R. H. Jordan, T. M. Miller, R. E. Slusher, and J. M. Philips: J. Appl. Phys. **80** (1996) 6954.

14) K. Neyts: Appl. Surf. Sci. **244** (2005) 517.

15) S. Tokito, T. Tsutsui, and Y. Taga: J. Appl. Phys. **86** (1999) 2407.

16) J. Grüuner, F. Cacialli, and R. H. Friend: J. Appl. Phys. **80** (1996) 207.

17) H. Riel, S. Karg, T. Beierlein, W. Rieß, and K. Neyts: J. Appl. Phys. **94** (2003) 5290.

18) H. Kajii, T. Tsukagawa, T. Taneda, K. Yoshino, M. Ozaki, A. Fujii, M. Hikita, S. Tomaru, S. Imamura, H. Takenaka, J. Kobayashi, F. Yamamoto, and Y. Omori: Jpn. J. Appl. Phys. **41** (2002) 2746.

19) B. Wei, K. Furukawa, J. Amagai, M. Ichikawa, T. Koyama, and Y. Taniguchi: Semicond. Sci. Technol. **19** (2004) L56.

20) B. Wei, K. Furukawa, M. Ichikawa, T. Koyama, and Y. Taniguchi: Jpn. J. Appl. Phys. **44** (2005) 4248.

21) A. Chin and T. Y. Chang: J. Lightwave Technol. **9** (1991) 321.

Figure captions

Fig. 1. (a) Configuration of MOLEDs and (b) chemical structures of coumarin 6 and rubrene used as dopant light-emitters.

Fig. 2. Reflectivity of DBR consisting of several pairs of SiO_2/Ta_2O_5. The number of SiO_2 and Ta_2O_5 pairs range from 1 to 7.

Fig. 3. Relationship between current efficiency at 60 mA/cm^2 and number of SiO_2/Ta_2O_5 pairs of DBR.

Fig. 4. Absorption coefficients of coumarin-6-doped Alq_3 and rubrene-doped Alq_3 solid thin films.

Fig. 5. EL emission spectra measured at different angles for device A with a mode index of 4 and coumarin-6-doped Alq_3 EML device. (a) MOLED with 4 SiO_2 and Ta_2O_5 pairs of and (b) non cavity OLED.

Fig. 6. EL emission spectra measured at different angles for device B with a mode index of 5 and coumarin-6-doped Alq_3 EML device. (a) MOLED with 4 SiO_2 and Ta_2O_5 pairs of and (b) non cavity OLED.

Fig. 7. Angular dependence of EL spectra for (a) device A, (b) device B, and (c) device C. The number of the DBR is varied between 1 and 7.

Fig. 8. Coupling efficiency between MOLED and optical fiber with NA of 0.5.

Device A	Device B	Device C
MgAg (150nm)	MgAg (150nm)	MgAg (150nm)
LiF (0.4nm)	LiF (0.4nm)	LiF (0.4nm)
Alq_3 (22nm)	Alq_3 (50nm)	Alq_3 (40nm)
Coumarin6:Alq_3 (20nm)	Coumarin6:Alq_3 (20nm)	Rubrene:Alq_3 (20nm)
α-NPD (28nm)	α-NPD (75nm)	α-NPD (40nm)
ITO (100nm)	ITO (150nm)	ITO (100nm)
DBR (SiO_2/Ta_2O_5 1-6 pairs)	DBR (SiO_2/Ta_2O_5 1-7 pairs)	DBR (SiO_2/Ta_2O_5 1-6 pairs)
Glass substrate	Glass substrate	Glass substrate

(a)

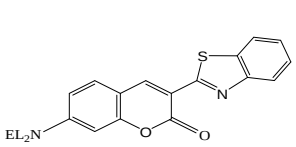

Coumarin6

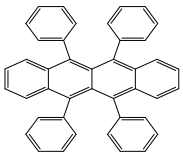

Rubrene

(b)

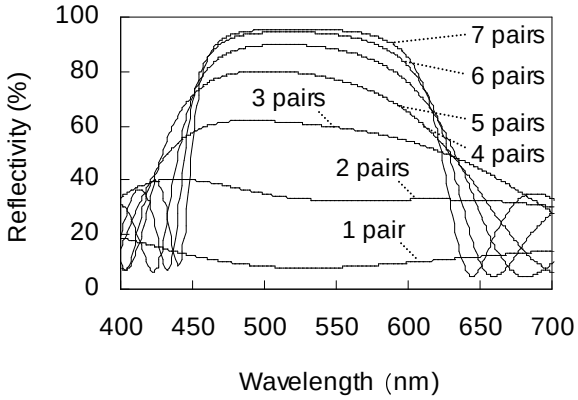
100
80
60
40
20
0
Reflectivity (%)
400
450
500
550
600
650
700
Wavelength（nm)
7 pairs
6 pairs
5 pairs
4 pairs
3 pairs
2 pairs
1 pair

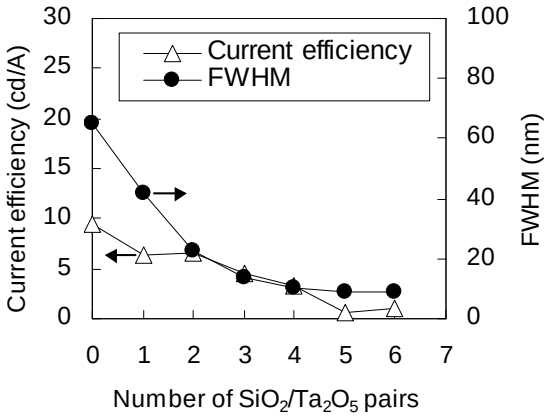
Current efficiency
FWHM
Current efficiency (cd/A)
FWHM (nm)
Number of SiO_2/Ta_2O_5 pairs

(a)

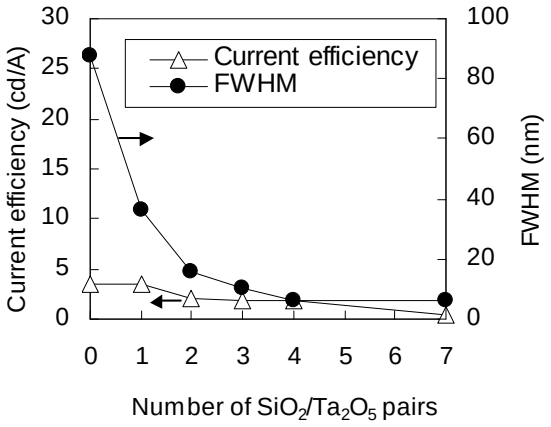
Current efficiency
FWHM
Current efficiency (cd/A)
FWHM (nm)
Number of SiO_2/Ta_2O_5 pairs

(b)

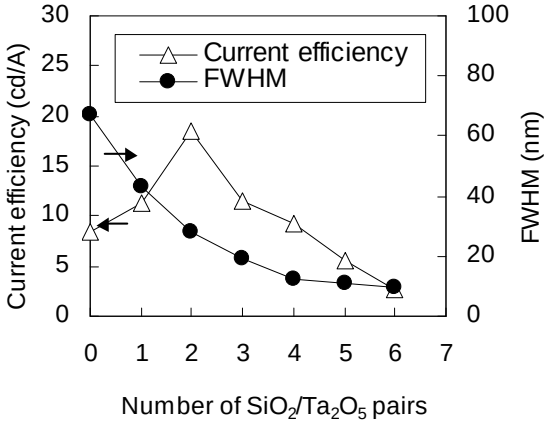
Current efficiency
FWHM
Current efficiency (cd/A)
FWHM (nm)
Number of SiO_2/Ta_2O_5 pairs

(c)

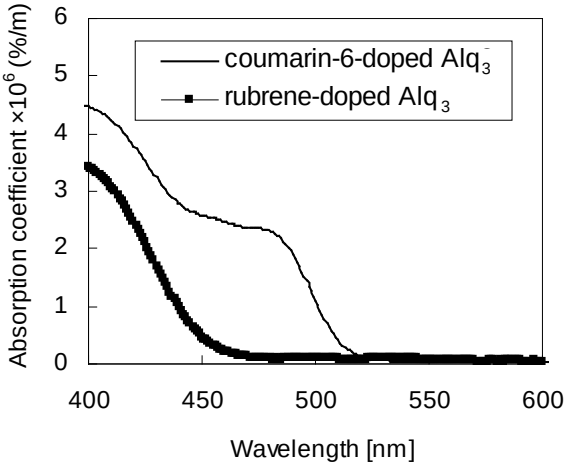
Absorption coefficient ×10^6 (%/m)
6
5
4
3
2
1
0
400
450
500
550
600
Wavelength [nm]
coumarin-6-doped Alq3
rubrene-doped Alq3

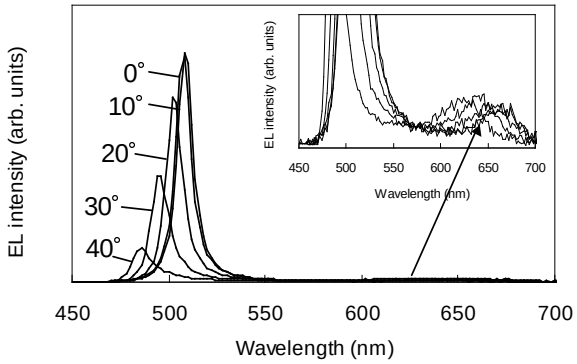
EL intensity (arb. units)
0°
10°
20°
30°
40°
EL intensity (arb. units)
450
500
550
600
650
700
Wavelength (nm)
450
500
550
600
650
700
Wavelength (nm)

(a)

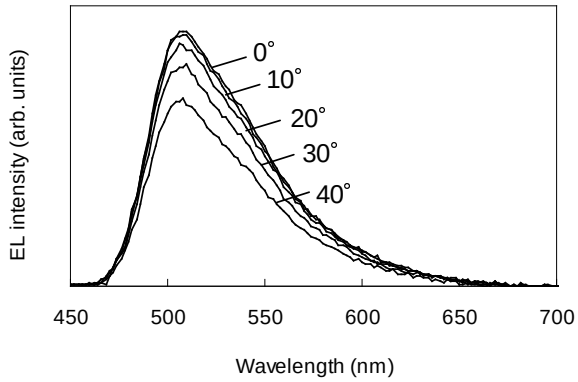
EL intensity (arb. units)
0°
10°
20°
30°
40°
450
500
550
600
650
700
Wavelength (nm)

(b)

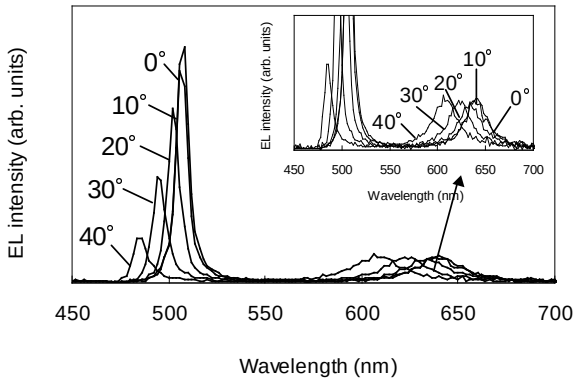
EL intensity (arb. units)
0°
10°
20°
30°
40°
450
500
550
600
650
700
Wavelength (nm)
EL intensity (arb. units)
10°
30°
20°
40°
0°
450
500
550
600
650
700
Wavelength (nm)

(a)

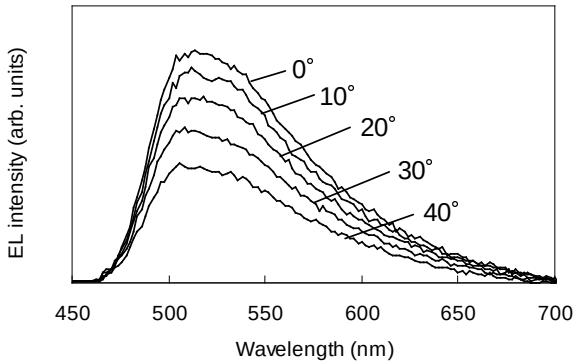
EL intensity (arb. units)
0°
10°
20°
30°
40°
450
500
550
600
650
700
Wavelength (nm)

(b)

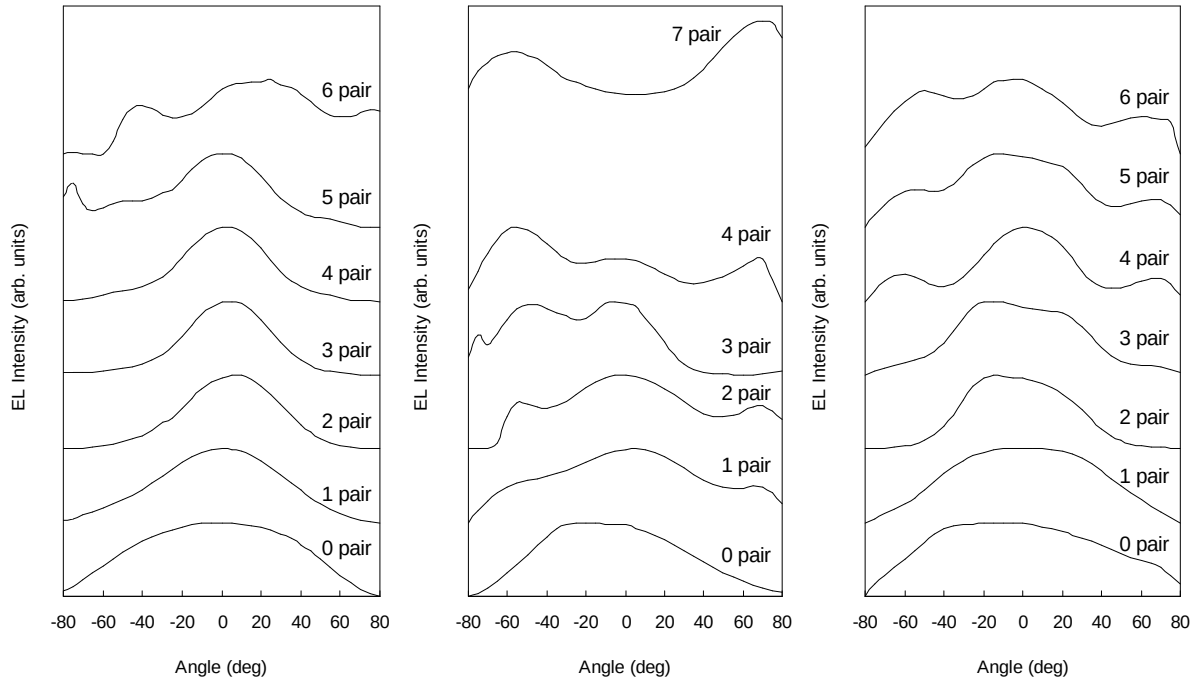
EL Intensity (arb. units)
6 pair
5 pair
4 pair
3 pair
2 pair
1 pair
0 pair
-80 -60 -40 -20 0 20 40 60 80
Angle (deg)
(a)
EL Intensity (arb. units)
7 pair
4 pair
3 pair
2 pair
1 pair
0 pair
-80 -60 -40 -20 0 20 40 60 80
Angle (deg)
(b)
EL Intensity (arb. units)
6 pair
5 pair
4 pair
3 pair
2 pair
1 pair
0 pair
-80 -60 -40 -20 0 20 40 60 80
Angle (deg)
(c)

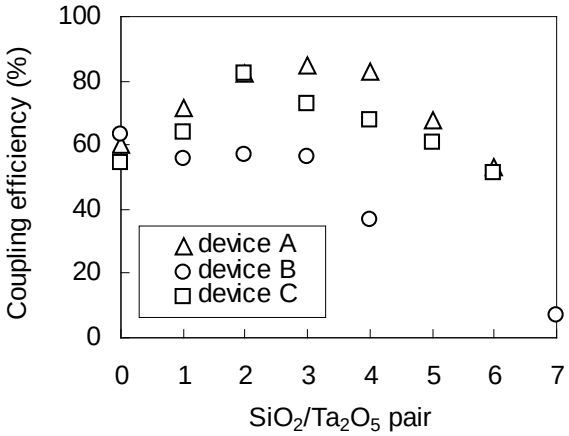
100
80
60
40
20
0
Coupling efficiency (%)
device A
device B
device C
0
1
2
3
4
5
6
7
SiO2/Ta2O5 pair